

Droplets sliding on soft solids shed elastocapillary rails

Nan Xue,^{1,2,3} Lawrence A. Wilen,⁴ Robert W. Style,^{1,*} and Eric R. Dufresne^{1,2,3,†}

¹*Department of Materials, ETH Zürich, 8093 Zürich, Switzerland.*

²*Department of Materials Science and Engineering, Cornell University, Ithaca, NY, 14853, USA.*

³*Laboratory of Atomic and Solid-State Physics, Cornell University, Ithaca, NY, 14853, USA.*

⁴*Center for Engineering Innovation and Design, School of Engineering and Applied Sciences, Yale University, NH, 06520, USA*

(Dated: September 4, 2024)

The surface tension of partially wetting droplets deforms soft substrates. These deformations are usually localized to a narrow region near the contact line, forming a so-called ‘elastocapillary ridge.’ When a droplet slides along a substrate, the movement of the elastocapillary ridge dissipates energy in the substrate and slows the droplet down. Previous studies have analyzed isotropically spreading droplets and found that the advancing contact line ‘surfs’ the elastocapillary ridge, with a velocity determined by a local balance of capillary forces and bulk rheology. Here, we experimentally explore the dynamics of a droplet sliding across soft substrates. At low velocities, the contact line is nearly circular, and dissipation increases logarithmically with speed. At higher droplet velocities, the contact line adopts a bullet-like shape, and the dissipation levels off. At the same time, droplets shed a pair of ‘elastocapillary rails’ that fade away slowly behind it. These results suggest that droplets favor sliding along a stationary ridge over surfing atop a translating one.

I. INTRODUCTION

A liquid droplet placed on a soft substrate induces the formation of an elastocapillary wetting ridge along its contact line [1–7]. These ridges arise from the interplay between capillary forces and the substrate’s elastic response. They are localized within a narrow region with a characteristic height of γ/E , where γ represents the surface tension of the droplet and E Young’s modulus of the soft substrate. For example, a water droplet on a gel with an elastic modulus of $O(10)$ kPa will typically form ridges with heights of $O(10)$ μm .

Previous studies [8–17] have shown that formation of an elastocapillary ridge underneath a moving contact line introduces dissipation within the substrate, slowing it down. This phenomenon is called ‘viscoelastic braking’. Two-dimensional models integrating capillarity and viscoelasticity have been successful in quantifying the dissipation associated with viscoelastic braking for isotropically spreading droplets [10–12, 14–17]. Essentially, ridge formation and relaxation generate a drag force per unit length of the contact line that increases with velocity, up to a limiting value comparable to the surface tension. Beyond this point, the contact line detaches from the elastocapillary ridge, leading to stick-slip motion.

For sliding droplets, the situation is more complex. Directional shear stresses that drive sliding break symmetry and deform the droplet [18–20]. Now, we expect feedback between the contact line dissipation and the global shape of the droplet. This competition plays out across a wide range of length scales, from the micron-scale structure of the elastocapillary ridge, to the millimeter-scale shape of the droplet.

In this paper, we apply interferometry to measure sub-micron deformations across millimeter-scale sliding droplets while simultaneously quantifying global dissipation, through drag force. At low velocities, the contact line is nearly circular, and drag increases logarithmically

with speed. At higher velocities, the drag force plateaus as the contact line becomes bullet-shaped. Strikingly, we also observe a pair of parallel ridges, which we call ‘elastocapillary rails,’ that gradually fade behind the droplet. The formation of elastocapillary rails is indicative of feedback between the microscopic elastocapillary ridge and the macroscopic droplet shape.

II. EXPERIMENTAL METHODS

We employ an interferometric platform [21] to simultaneously investigate the interplay between macroscopic droplet shape, microscopic elastocapillary ridge formation and relaxation, and the associated energy dissipation during droplet motion on soft substrates. Figure 1(a) and Movie 1 depict the side view of the platform, while Fig. 1(b) provides a schematic representation (optical paths detailed in Ref. 21 and Fig. S1 in ESI).

A. Experimental setup

An aqueous liquid bridge is formed between a capillary (outer diameter $D = 1.2$ mm) and a soft substrate [Fig. 1(b)]. We refer to this as a ‘droplet’ for the rest of the paper. The capillary connects to a water reservoir through silicone rubber tubing, allowing us to maintain a constant positive pressure difference ($\Delta p = 100$ Pa) between the interior of the droplet and the surrounding atmosphere. This compensates for the water evaporation, enabling experiments using pure water instead of ionic liquids [22].

Two silicone materials with differing stiffnesses are used as substrates: a stiffer elastomer (Sylgard 184, 10:1, $E = 600$ kPa) and a softer gel (Dow Corning CY52-276, 1:1, $E = 4$ kPa) [21]. Both exhibit similar macroscopic wetting properties with a surface tension $\gamma_s \approx 30$

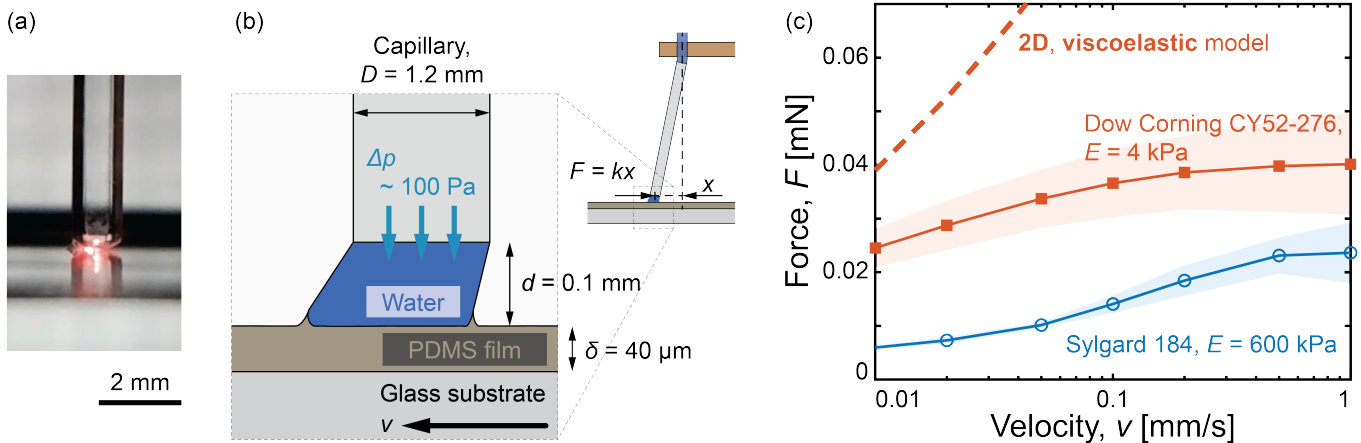


FIG. 1. The platform for studying droplet motion on soft substrates. (a) Side view of the droplet between the capillary and the substrate; see also in Movie 1. (b) Schematic of the experimental setup. (c) The measured force F as a function of the droplet velocity v . The colored shadow represents the standard deviation across three experiments on different samples.

mN/m [21]. Following Refs. 10, 21, the complex modulus of the softer gel is modeled by the power-law form $G^*(\omega) = G_0[1 + (i\omega\tau)^n]$ with shear modulus $G_0 = 1.3$ kPa, intrinsic timescale $\tau = 0.11$ s, and power $n = 0.54$. We prepare uniform $40 \mu\text{m}$ thick gel films by spin-coating uncured silicone (five drops from a 3 mL pipette, one minute at 800 rpm) onto glass substrates, followed by curing at 40°C over 25 hours. In our experiments, we observed no discernible effects attributable to a potentially uncured gel [23].

The droplet height is set at $d = 0.1$ mm by controlling the capillary-substrate distance. Motorized actuators (Thorlabs, Z812B and ZST213B) control the lateral positions of the capillary and substrate, respectively, each enabling relative velocities between $v = 0.01$ mm/s and $v = 1$ mm/s. For high-accuracy dissipation measurements, the base of the capillary is stationary while the substrate moves at the velocity, v . Conversely, to measure substrate deformation via interferometry, the substrate is stationary, and the base of the capillary moves at the velocity, v . This setup allows for precise control of the droplet's velocity and measurement of its response. Throughout this manuscript, we report data only for droplets in a steady state, ensuring they have been translated at least 2 mm from their initial position.

B. Force and Deformation Measurements

Similar to Refs. 22, 24, the displacement of the capillary tip (x) responds linearly to the force (F) acting on the sliding droplet [Fig. 1(b)]. To calibrate the spring constant, k , we re-orient the capillary horizontally, bring its tip in contact with a balance, and record the force response to vertical displacements (details in Fig. S2 in ESI). By adjusting the capillary and tubing geometry, we maintain $k \approx 0.1$ mN/mm throughout our experiments. Figure 1(c) presents typical force measurements

as a function of droplet velocity.

We employ a Linnik interference imaging setup to quantify soft substrate deformation [21, 25]. An LED light source ($\lambda = 643$ nm) illuminates the substrate from below, and reflected light from the water-substrate interface interferes with a reference beam. Figure 2 displays typical captured patterns. These interference patterns, when processed with phase retrieval methods, enable high-resolution analysis of substrate deformation on the order of 1 nm (details and demo code in ESI). Additionally, the interferometric imaging simultaneously captures droplet shapes (dark shadows, Fig. 2) and capillary positions (shallow shadows, Fig. 2).

III. EXPERIMENTAL RESULTS AND DISCUSSIONS

A. Force measurements

Figure 1(c) shows direct measurements of the drag force F experienced by a droplet moving on a soft substrate as a function of droplet velocity, v . Data for 4 kPa silicone gels and 600 kPa silicone elastomers are shown as filled red squares and hollow blue circles, respectively. Consistent with previous work on viscoelastic braking, the drag force is significantly higher on the softer substrate and increases with velocity. Interestingly, at higher velocities, the drag force levels off. We note that the drag force is directly connected to the energy dissipation rate, which is $P = Fv$, shown in Fig. S3 in ESI.

We compare these results to a viscoelastic model of an isotropically spreading droplet on a deformable substrate [10]. After substituting the wetting and rheological properties of our softer gel into the model, and twice the resting diameter of the droplet as an approximation for the length of the contact line (details in ESI; ‘twice’ is to account for both advancing and receding fronts, with

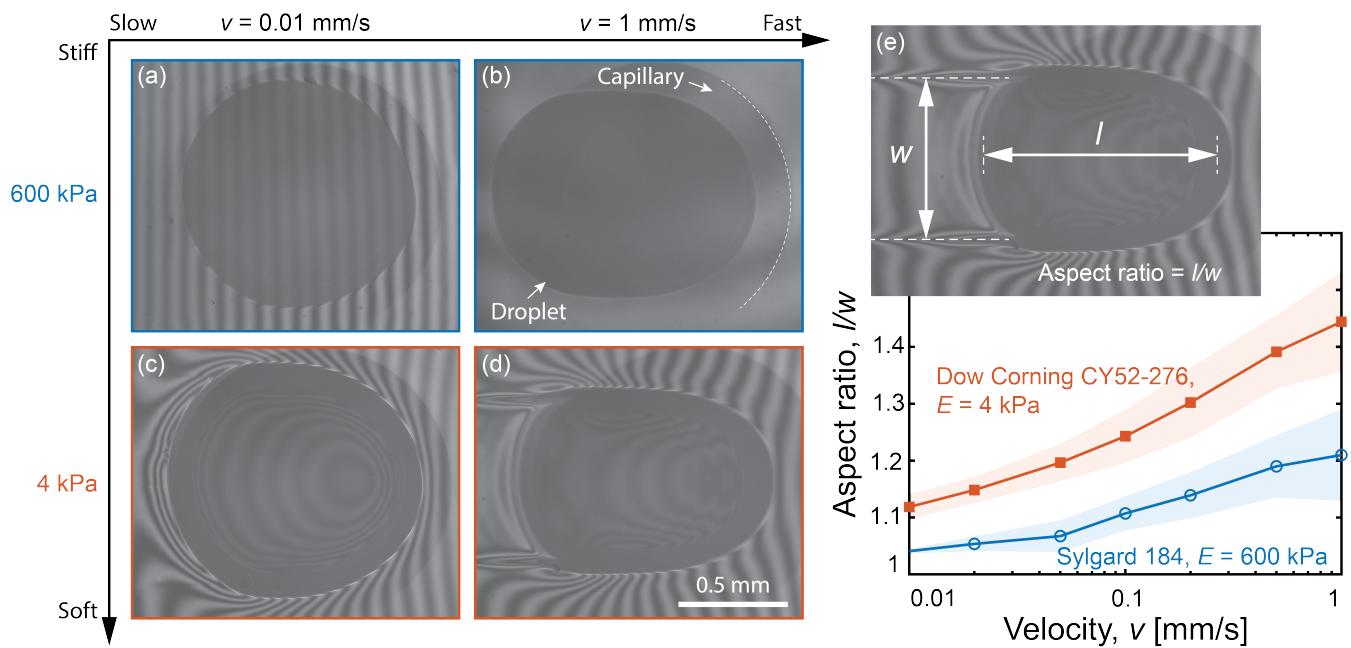


FIG. 2. Droplet shapes on substrates with different elasticities and sliding velocities (see Movies 2-5). Images show droplets on stiffer ($E = 600$ kPa, panels a, b) and softer ($E = 4$ kPa, panels c, d) gels. Droplet velocity increases from left to right. (e) Aspect ratio (l/w) as a function of velocity, demonstrating greater shape change on the softer substrate. The colored shadow represents the standard deviation across three experiments.

further discussion of the choice of the contact line size in Section III B), we obtain a theoretical prediction for the drag on the droplet on the softer gel, shown as dashed red line in Fig. 1(c). This prediction overestimates the experimentally measured drag.

B. Droplet shapes

While the model prediction in Section III A conveniently used twice the resting droplet diameter as an approximation for contact line size, Refs. 18, 20 emphasize that droplets can undergo significant shape changes during sliding. Our experiments confirm this, especially at higher velocities on softer substrates. Typical droplet shapes captured by interferometric imaging during sliding from left to right are shown in Fig. 2 (dark shadows represent the droplets).

At lower velocities, droplets on both softer and stiffer gels maintain a nearly circular contact line [Figs. 2(a, c)]. However, at higher velocities, the contact line elongates in the direction of motion and narrows in the transverse direction [Figs. 2(b, d)]. This reshaping is particularly pronounced on softer gels, where the droplets take on a bullet-like form: The contact lines become straight and parallel to the direction of motion. We quantify this reshaping by measuring the droplet's length, l , and width, w [Fig. 2(e)]. The aspect ratio, l/w , increases with velocity on both gels, with a larger shape change on the softer gel. This increase in the aspect ratio is mainly driven

by the change in the droplet width, as the change in the length of the droplet is minor (detailed measurements in Fig. S4 in ESI).

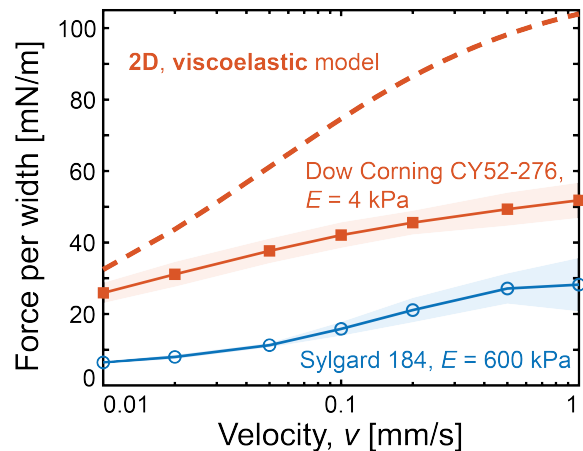


FIG. 3. The measured force per unit width of the moving droplet as a function of velocity v . The colored shadow represents the standard deviation across three experiments.

Despite the confinement in the narrow gap between the capillary and the substrate, we observe a decrease in droplet width with increasing velocity (detailed measurements in Fig. S5 in ESI). This suggests that using dynamic droplet width, rather than its size at rest, is a

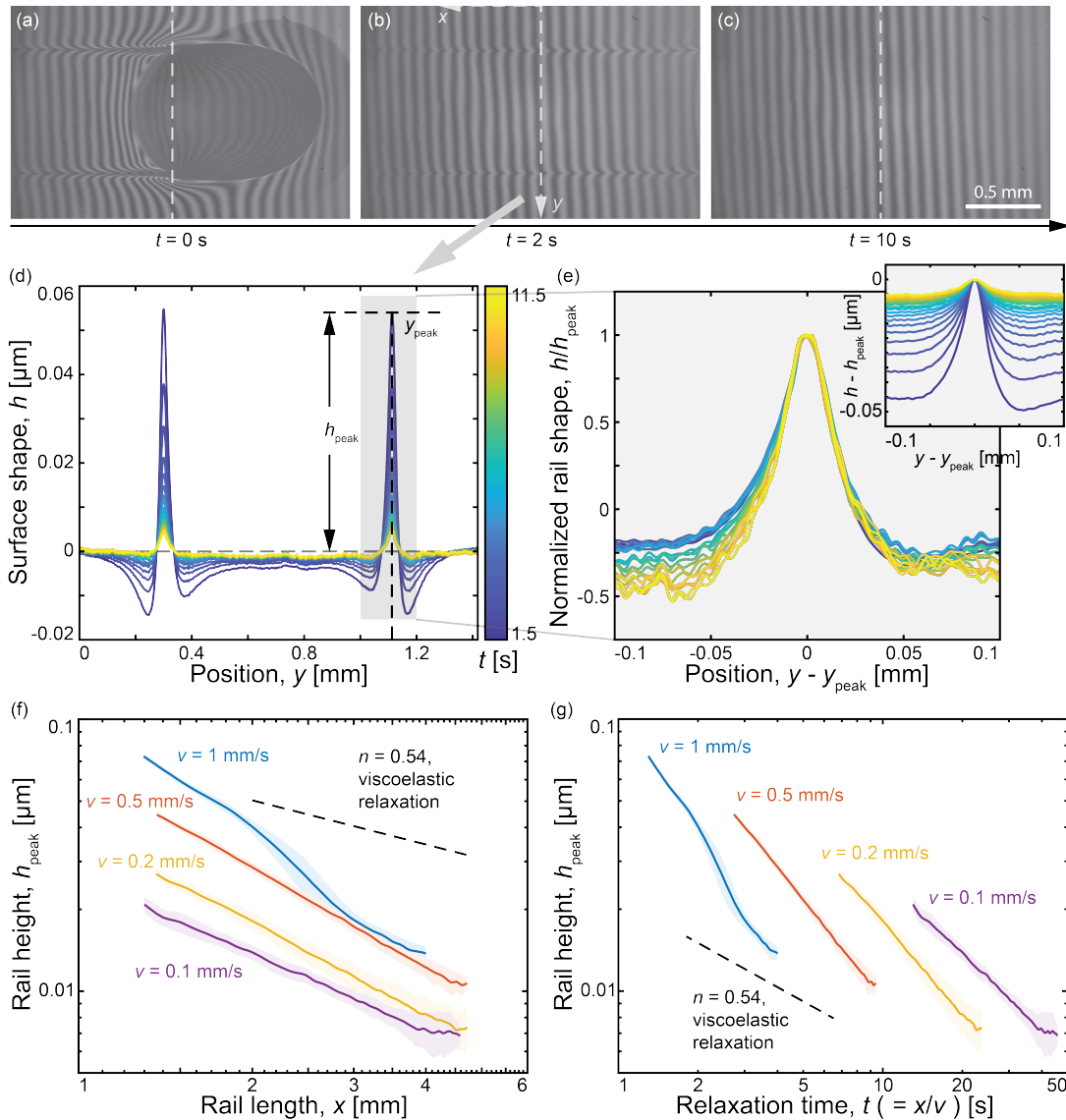


FIG. 4. The relaxation of the elastocapillary rails. (a-c) Interferometric images showing the time evolution of the deformed substrate: $t = 0$ s (a), 2 s (b), and 10 s (c). The corresponding movie is Movie 6. (d) The relaxation of the substrate (h) along the vertical dashed line in (a-c). (e) Zoom-in profile of the rails near their tips. The rail shape is normalized by its peak height, h_{peak} . The inset shows the rail profile (height difference from the peak, $h - h_{\text{peak}}$) as a function of $y - y_{\text{peak}}$. (f) Relaxation of the rail height h_{peak} as a function of the length along the rail, x . (g) Relaxation of the rail height h_{peak} over time, t . The colored shadow shows the standard deviation (details in Fig. S5 in ESI).

more accurate way to characterize the size of the contact line involved in energy dissipation. Accordingly, we calculate the drag per unit width by dividing the measured force by twice the droplet width, Fig. 3. By considering the droplet shape change, the experimental data moves closer (but certainly not collapsing) to the 2D linear viscoelastic model prediction (dashed red line in Fig. 3), particularly at low velocities.

A key difference between our experiment and the 2D model is that the model assumes straight contact lines perpendicular to the direction of motion. Sliding droplets, however, involve curved contact lines with a sig-

nificant velocity component parallel to them. Nevertheless, the existing 2D model provides satisfactory order-of-magnitude estimations for dissipation [22]. Simple extensions of this model accounting for finite substrate thickness and circular contact line shape (ESI) result in a negligible change to the predicted dissipation.

C. Elastocapillary Rails

At high speeds, droplets not only assume a bullet-like morphology, but they also leave behind an unusual pair

of parallel rails. These structures are clearly visible in our interferometric images [Figs. 2(c, e), Fig. 4(a), and Movies 5 and 6]. They appear as a pair of parallel deformations to interferometric fringes following the direction of the droplet motion, and connecting to its sides. These fringes indicate surface topography, which we quantify using phase retrieval methods described in Refs. 26–28 (details in ESI). This method achieves a remarkably high out-of-plane resolution on the order of 1 nm. The resulting profile, shown in Fig. 4(d), reveals a pair of parallel ridges we term ‘elastocapillary rails.’ These rails can reach up to $O(1)$ mm in length. They are tallest near the droplet, with a height of $O(100)$ nm from the rear of the droplet. Interferometry does not allow measurements closer to the contact line because steep profiles prevent resolution of the fringes.

The shape of the elastocapillary rails shares some features with typical wetting ridges, in the absence of a contact line. Analyzing the deformed surface shape along a vertical line in the interferometric images [Figs. 4(a–c)] reveals their cross-sectional profile [Fig. 4(d)]. They have a width of about $50 \mu\text{m}$, compared to the elastocapillary length of $\gamma/E \approx 10 \mu\text{m}$, and ‘dimples’ on either side that are known to appear when the substrate thickness becomes comparable to the elastocapillary length [29]. In contrast to wetting ridges, however, the tips of the rails are rounded [21, 30] rather than triangular [29]. Notably, the rails extend beyond the immediate vicinity of the contact line and detach from the droplets. Finally, the shape of the tips of these wetting ridges evolves over time in a self-similar fashion. If we shift the tips of the rails at different times, we see that their shapes do not overlap [inset in Fig. 4(e)]. Instead, the slopes along the sides and the curvatures at the tip decrease over time or distance from the droplet. However, scaling the rail cross-section by its height collapses the profiles at different locations/times [Fig. 4(e)]. Self-similar evolution is consistent with the viscoelastic relaxation model [10].

We quantify the rail height (h_{peak}) [Fig. 4(d)] as a function of distance from the droplet, x . Rails are more prominent at higher droplet velocities, as shown in Fig. 4(f). Conversely, Fig. 4(g) displays the relaxation of the height as a function of time since it was shed from the sliding droplet. Here, lower droplet velocities result in longer rail persistence.

IV. DISCUSSION AND CONCLUSIONS

Our interferometric platform enabled simultaneous investigation of multiscale structure and dynamics of

droplets sliding on a deformable substrate. At higher droplet velocities, droplets adopt a distinct bullet-like shape, the drag force levels off, and prominent parallel elastocapillary rails are shed from the droplet. Feedback between the microscopic structure of the elastocapillary ridge and the overall shape of the droplet plays an essential role in these phenomena. Sliding along a wetting ridge creates much less drag than surfing across it. This favors the narrowing of the droplet, creating longer droplets. At high speeds, the length of the parallel side contact lines of the bullet-like droplets is similar to the droplet length, l .

Points along the sides of a sliding droplet are pulled upward by the liquid-vapor interface for a time $O(l/v)$ while points at the front and back of the droplet are only pulled upward for a time $O(\gamma/Ev)$. Thus, the ridges on the side of the droplet are loaded by a factor of $EL/\gamma = O(100)$ longer than the front. Previous work [21, 31] shows that poroelasticity can lead to a ridge decay-time comparable to the time of contact between the droplet and substrate. Thus, elastocapillary ridges formed along the direction of motion would be more persistent, than those at the leading and trailing edges of the droplet. This leads to the formation of sheddable elastocapillary rails. The relaxation data in Fig. 4(g) supports this hypothesis, as rails formed at low speeds (*i.e.*, long contact times) take longer to decay.

Further evidence for poroelastic contributions can be found in the rail height as a function of time, shown in Fig. 4(g). A purely viscoelastic model would predict $h \propto t^{-n}$, where $n = 0.54$ based on the rheology of our gel [dashed line in Figs. 4(f, g)]. However, we observe a steeper power-law relaxation, consistent with Ref. 21.

Our results underscore the need for scale-crossing models that link contact line dissipation to overall droplet shape [32], incorporating elements of both viscoelasticity [10] and poroelasticity [31].

AUTHOR CONTRIBUTIONS

N.X. and E.R.D. conceptualized the research. N.X. and L.A.W. designed the experimental setup. N.X. performed the experiments and processed the data. N.X., L.A.W., R.W.S., and E.R.D. discussed the results and wrote the paper.

CONFLICTS OF INTEREST

There are no conflicts to declare.

* robert.style@mat.ethz.ch

† eric.r.dufresne@cornell.edu

[1] M. E. R. Shanahan and A. Carre, Anomalous spreading of liquid drops on an elastomeric surface, *Langmuir* **10**, 1647 (1994).

- [2] M. E. R. Shanahan and A. Carre, Viscoelastic dissipation in wetting and adhesion phenomena, *Langmuir* **11**, 1396 (1995).
- [3] R. Pericet-Cámara, A. Best, H.-J. Butt, and E. Bonaccorso, Effect of capillary pressure and surface tension on the deformation of elastic surfaces by sessile liquid microdrops: an experimental investigation, *Langmuir* **24**, 10565 (2008).
- [4] A. Jagota, D. Paretkar, and A. Ghatak, Surface-tension-induced flattening of a nearly plane elastic solid, *Phys. Rev. E* **85**, 051602 (2012).
- [5] R. W. Style, A. Jagota, C.-Y. Hui, and E. R. Dufresne, Elastocapillarity: Surface tension and the mechanics of soft solids, *Annu. Rev. Condens. Matter Phys.* **8**, 99 (2017).
- [6] A. Bardall, K. E. Daniels, and M. Shearer, Deformation of an elastic substrate due to a resting sessile droplet, *Eur. J. Appl. Math.* **29**, 281 (2018).
- [7] B. Andreotti and J. H. Snoeijer, Statics and dynamics of soft wetting, *Annu. Rev. Fluid Mech.* **52**, 285 (2020).
- [8] A. Carré, J.-C. Gastel, and M. E. R. Shanahan, Viscoelastic effects in the spreading of liquids, *Nature* **379**, 432 (1996).
- [9] D. Long, A. Ajdari, and L. Leibler, Static and dynamic wetting properties of thin rubber films, *Langmuir* **12**, 5221 (1996).
- [10] S. Karpitschka, S. Das, M. van Gorcum, H. Perrin, B. Andreotti, and J. H. Snoeijer, Droplets move over viscoelastic substrates by surfing a ridge, *Nat. Commun.* **6**, 7891 (2015).
- [11] M. Zhao, J. Dervaux, T. Narita, F. Lequeux, L. Limat, and M. Roché, Geometrical control of dissipation during the spreading of liquids on soft solids, *Proc. Natl. Acad. Sci. U.S.A.* **115**, 1748 (2018).
- [12] M. van Gorcum, B. Andreotti, J. H. Snoeijer, and S. Karpitschka, Dynamic solid surface tension causes droplet pinning and depinning, *Phys. Rev. Lett.* **121**, 208003 (2018).
- [13] H. Liang, Z. Cao, Z. Wang, and A. V. Dobrynin, Surface stresses and a force balance at a contact line, *Langmuir* **34**, 7497 (2018).
- [14] M. van Gorcum, S. Karpitschka, B. Andreotti, and J. H. Snoeijer, Spreading on viscoelastic solids: are contact angles selected by neumann’s law?, *Soft Matter* **16**, 1306 (2020).
- [15] K. Smith-Mannschott, Q. Xu, S. Heyden, N. Bain, J. H. Snoeijer, E. R. Dufresne, and R. W. Style, Droplets sit and slide anisotropically on soft, stretched substrates, *Phys. Rev. Lett.* **126**, 158004 (2021).
- [16] D. Mokbel, S. Aland, and S. Karpitschka, Stick-slip contact line motion on kelvin-voigt model substrates, *Europhys. Lett.* **139**, 33002 (2022).
- [17] H. Jeon, Y. Chao, and S. Karpitschka, Moving wetting ridges on ultrasoft gels, *Phys. Rev. E* **108**, 024611 (2023).
- [18] T. Podgorski, M. Flesselles, J., and L. Limat, Corners, cusps, and pearls in running drops, *Phys. Rev. Lett.* **87**, 036102 (2001).
- [19] M. Oléron, *Dynamic wetting of viscoelastic substrates*, Ph.D. thesis, Université Paris Cité (2022).
- [20] M. Oléron, L. Limat, J. Dervaux, and M. Roché, Morphology and stability of droplets sliding on soft viscoelastic substrates, *Soft Matter* **20**, 762 (2024).
- [21] Q. Xu, L. A. Wilen, K. E. Jensen, R. W. Style, and E. R. Dufresne, Viscoelastic and poroelastic relaxations of soft solid surfaces, *Phys. Rev. Lett.* **125**, 238002 (2020).
- [22] H. K. Khattak, S. Karpitschka, J. H. Snoeijer, and K. Dalnoki-Veress, Direct force measurement of microscopic droplets pulled along soft surfaces, *Nat. Commun.* **13**, 4436 (2022).
- [23] A. Hourlier-Fargette, A. Antkowiak, A. Chateauminois, and S. Neukirch, Role of uncrosslinked chains in droplets dynamics on silicone elastomers, *Soft Matter* **13**, 3484 (2017).
- [24] C. Hinduja, H.-J. Butt, and R. Berger, Slide electrification of drops at low velocities, *Soft Matter* (2024).
- [25] A. Dubois, L. Vabre, A.-C. Boccara, and E. Beaurepaire, High-resolution full-field optical coherence tomography with a linnik microscope, *Appl. opt.* **41**, 805 (2002).
- [26] M. Takeda, H. Ina, and S. Kobayashi, Fourier-transform method of fringe-pattern analysis for computer-based topography and interferometry, *J. Opt. Soc. Am.* **72**, 156 (1982).
- [27] M. A. Herráez, D. R. Burton, M. J. Lalor, and M. A. Gdeisat, Fast two-dimensional phase-unwrapping algorithm based on sorting by reliability following a noncontinuous path, *Appl. Opt.* **41**, 7437 (2002).
- [28] M. F. Kasim, Fast 2D phase unwrapping implementation in MATLAB (2017).
- [29] R. W. Style, R. Boltyskiy, Y. Che, J. Wettlaufer, L. A. Wilen, and E. R. Dufresne, Universal deformation of soft substrates near a contact line and the direct measurement of solid surface stresses, *Phys. Rev. Lett.* **110**, 066103 (2013).
- [30] J. D. Berman, M. Randeria, R. W. Style, Q. Xu, J. R. Nichols, A. J. Duncan, M. Loewenberg, E. R. Dufresne, and K. E. Jensen, Singular dynamics in the failure of soft adhesive contacts, *Soft matter* **15**, 1327 (2019).
- [31] M. Zhao, F. Lequeux, T. Narita, M. Roché, L. Limat, and J. Dervaux, Growth and relaxation of a ridge on a soft poroelastic substrate, *Soft matter* **14**, 61 (2018).
- [32] N. Le Grand, A. Daerr, and L. Limat, Shape and motion of drops sliding down an inclined plane, *J. Fluid Mech.* **541**, 293 (2005).